About the excitation dependency of risk tolerance mapping in dynamically loaded structures

A. Zanarini
University of Bologna, Department of Industrial Engineering,
Viale Risorgimento 2, I-40136, Bologna, Italy
e-mail: **a.zanarini@unibo.it**

Abstract

To demonstrate the viability of this risk tolerance concept, accurate ESPI-based *receptance* maps' estimations of the experimental structural dynamics of a lightweight rectangular plate were here used, with two distinct excitation sources. ESPI technology actually permits a precise estimation of superficial strain FRF maps, which, with the aid of a constitutive model of the material and of a fatigue method for duration prediction, can lead to frequency-to-failure maps, as function of the specific excitation location and signature. Once a proper risk index and its acceptance threshold are formulated, the risk index maps can grade the failure risk as function of the real structural dynamics and boundary conditions of the real component, of the excitation location and of its dynamic signature. Examples and details are given specifically as the excitation changes location, in order to show how the most advanced experiment-based knowledge available can augment the fidelity of the proposed risk tolerance and defect acceptance mapping.

1 Introduction

In seeking the absolute failure safety of dynamically loaded structures, most of the times defects are simplistically not allowed. This has a strong reflection on the manufacturing and maintenance costs, but hides a lack of knowledge and trust about the real structural dynamics of the components, of the real boundary conditions and of the excitation signatures. Instead, a more precise knowledge of the structural responses to specific dynamic loads, coupled with advanced failure prediction models for cumulative damage, may lead to the concept of risk tolerance and sub-condition defect acceptance, therefore mapping the specific failure risk in the component body and grading, with a proper risk index, the danger of each defect as function of the position where it may occur. In this risk tolerance and defect acceptance perspective, using higher knowledge in structural dynamics, only the defects that lay in the risk index maps above a specific threshold level should be avoided, therefore permitting the usage of defected components only if the defects are revealed in the areas below the risk index level for that specific task, saving costs in complex manufacturing and maintenance.

The viability of this risk tolerance concept can be demonstrated by means of accurate *receptance* maps' estimations of the experiment-based structural dynamics. The sample here used was a lightweight rectangular plate, with two distinct excitation sources; its dynamics was measured using the Dynamic ESPI technology, in a broad frequency band, without any structural FE models to be accurately tuned, exploiting the results of the fundamental research project TEFFMA, funded by the European Commission and carried out by the author[1] at the Vienna University of Technology. TEFFMA aimed at making a comparison between the state-of-the-art in native full field optical technologies and the SLDV as reference, to understand at which point of their development these experimental procedures can provide NVH applications with enhanced peculiarities. It is important to remark how these works were based on non-contact measurements, without structural dynamics distortions, resulting in a dense grid of sensing locations, which are relevant for a broad frequency band experimental vibration model with accurate spatial description for complex pattern identification and,

[1] A. Zanarini, scientific proposer & experienced researcher in the project TEFFMA - Towards Experimental Full Field Modal Analysis, financed by the Marie Curie FP7-PEOPLE-IEF-2011 PIEF-GA-2011-298543 grant, 1/02/2013 - 31/07/2015.

furthermore, for experimental dynamic model of strains, stresses & failure criteria, accurate maps of cumulative damage distributions for fatigue life assessment, defect tolerance criteria and risk index based only on full-field testing in production & working conditions.

Although these works are a spin-off of the activities held during the TEFFMA project, they find their roots in the HPMI-CT-1999-00029 *Speckle Interferometry for Industrial Needs* Post-doctoral Marie Curie Industry Host Fellowship project at Dantec Ettemeyer GmbH. Since the testing in the latter (see [1, 2]) it became self-evident how ESPI measurements could give relevant mapping about the local behavior for enhanced structural dynamics assessments (see [3]) and fatigue spectral methods (see [4, 5]). The results in the former were the basis for the TEFFMA birth, whose works saw earlier presentations in [6, 7], followed by [8–11]. In [12] a gathering of the works of TEFFMA was firstly attempted, while in [13] an extensive description of the whole *receptance* testing was faced and in [14] the EFFMA was detailed together with model updating attempts. The works in [15] underlined the quality of ESPI datasets in full-field dynamic testing. In [16] a precise comparison was made about new achievements for *rotational* and *strain FRF* high resolution experiment-based *maps*. As described, many works [4–14] were already published by the author about the growing full-field optical technologies, their advantages and drawbacks in a broad frequency range. It was shown, especially in the latest works [6,9,12–14,16] from the TEFFMA project, how the growing native full field techniques have started to offer tangible advances for the consistency and continuity of their data fields, with clear repercussions in model updating and derivative calculations (*rotational dofs* and *strains*). About the latter, the reader can appreciate in [9, 12, 16] the effect of the measurement noise; though, unfortunately due to the complexity or burden of their measurement, the *rotational dofs* are usually disregarded, whilst they are relevant for the successful build of a reliable dynamic model for complex structures [17–21].

In [12, 16] was previously underlined how ESPI technology actually permits one of the most accurate sensing of experiment-based structural dynamics for the evaluation of superficial *strain FRF maps*. The latter can lead to frequency-to-failure maps, as function of the specific excitation dynamic signature and energy injection location, exploiting a proper constitutive model of the material and a fatigue spectral method, here the Dirlik's one [22]. It becomes then possible to define a proper risk index and its threshold, based on the frequency-to-failure maps. Therefore the risk index maps can grade the failure risk, as function of the real structural dynamics and boundary conditions of the specific component; but also as function of the excitation's location and spectrum. In [23] the risk index was introduced as a metric to distinguish failure-exposed areas in a dynamically loaded component, with a focus also on the evidences from a damaged fiberglass reinforced composite panel [24]. In the recent paper [25] the variability of risk maps was analysed by the changes in the excitation dynamic signature.

Here, instead, the focus is on the behavioral change of the risk index maps due to excitation location, in order to highlight the relevance an accurate test-based structural dynamics plays in durability evaluations. As in the TEFFMA project 2 distinct shakers were available, the *receptance* maps were acquired from both, also to enhance the EFFMA as in [14], with broad frequency band excitation. Therefore the *experiment-based full-field FRF approach* can bring the complete & real structural dynamics, as subjected to 2 different loading locations, into fatigue life predictions, therefore assessing the proposed risk tolerance strategy as the excitation/loading is varied in the energy injection point. In such a broad perspective, for the retained dynamics and for the high resolution mapping achievable, the location of the potential defect plays an uttermost relevance in the crack & failure start: what follows is devoted to highlight the potentials of this smart approach with simple examples. Examples and details are given specifically as the excitation is changed in location, in order to show how the most advanced experiment-based knowledge available can augment the fidelity of the proposed risk tolerance and defect acceptance mapping.

A recall of the experiment-based FRF modeling is sketched in Section 2. A brief description of the testing is outlined in Section 3, with attentions on the setup. Section 4 deals with the numerical derivation of strain and stress fields from *receptance* maps, which are relevant to the cumulative damage spectral methods in Section 5. Section 6 pertains the definition of a defect tolerance scheme, before Section 7 for the final conclusions.

2 Full Field FRFs: direct experimental modelling

All the activities in the TEFFMA project gravitate around impedance-based studies by means of full-field optical measurements, in order to obtain highly reliable Full-Field FRFs with unprecedented spatial resolutions, for any further speculation that may come either from experimental test or from numerical models, also in hybrid frameworks.

2.1 Brief recall of a direct characterisation

The well known formulation [17,20] of *receptance* matrix $\boldsymbol{H_d}(\omega)$, as spectral relation between displacements and forces, will be used for the Full-Field FRF estimation, describing the dynamic behaviour of a testing system, with potentially multi-input excitation, here 2 distinct shakers, and *many*-output responses, here also several thousands covering the whole sensed surface, as can be formulated in the following complex-valued equation:

$$H_{d_{ij}}(\omega) = \frac{\sum_{k=1}^{N} S^k_{X_i F_j}(\omega)}{\sum_{k=1}^{N} S^k_{F_j F_j}(\omega)} \in \mathbb{C} \tag{1}$$

where X_i is the output displacement at *i*-th dof induced by the input force F_j at *j*-th dof, while $S^k_{X_i F_j}(\omega)$ is the k-th cross power spectral density between input and output, $S^k_{F_j F_j}(\omega)$ is the k-th auto power spectral density of the input and ω is the frequency, evaluated in N repetitions.

Once the specific excitation signature $F_j(\omega)$ is known in the frequency domain, the FRF formulation in Eq.1 can be used to obtain the full-field displacements over the entire surface, as follows at specific output dof i:

$$d_{ij}(\omega) = H_{d_{ij}}(\omega) F_j(\omega) \in \mathbb{C} \tag{2}$$

or for the whole displacement vector $\boldsymbol{d}_j$ due to the excitation in dof j as:

$$\boldsymbol{d}_j(\omega) = \boldsymbol{H_d}_j(\omega) F_j(\omega) \in \mathbb{C} \tag{3}$$

Increasing the spatial resolution in dynamic models by means of many dofs Full-Field FRFs will be therefore a valuable addition to the state-of-the-art of the design of complex systems and will surely lead to the exploration of new FRF-based quantities derived from excellent quality displacement fields, such as surface rotations, strains & stresses and failure point distributions [9–12, 14, 16]. Furthermore, distributed loading patterns, such as those coming from vibro-acoustics [26], might be considered.

3 Activities in the lab of TU-Wien for the TEFFMA project

The well equipped laboratory of the TU-Wien made possible a complex set-up for the comparison of the qualities of three different technologies available in acquiring Full-Field FRFs (as best detailed in [13]): SLDV, Hi-Speed DIC and Dynamic ESPI.

3.1 Summary of the technological equipment

During the time of the measurements the laboratory facility at TU-Wien had a dedicated room with seismic floor and air-cushion anti-vibration optical table, to filter out the environmental vibrations. A Polytec PSV 300 was at disposal, with the 1D (out-of-plane) scanning head OFV-056. Due to its peculiarities of being the junction instrument between the traditional NVH measurement technologies and the growing native full-field equipment, SLDV was taken as reference. Besides, it must be recalled that SLDV delivers velocities and not displacements. The native full-field equipment consisted in the Dantec Ettemeyer Q-500 Hi-Res, the ESPI

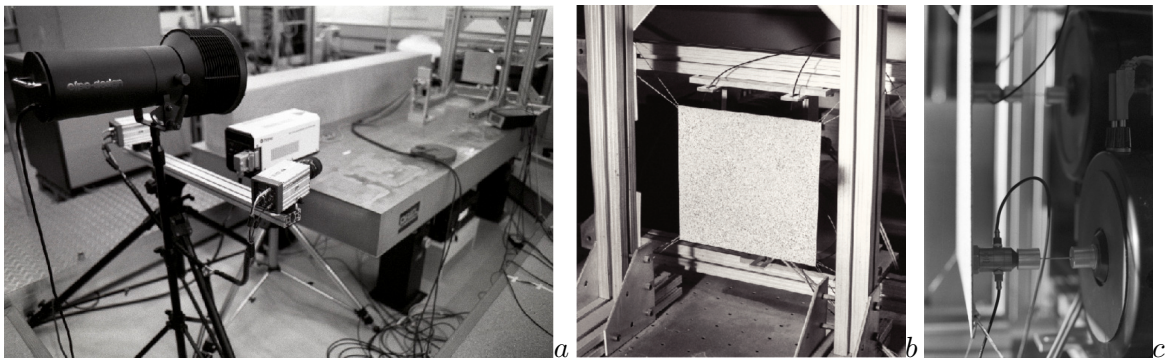

Figure 1: Full field measurement instruments gathered in front of the specimen at the optical anti-vibration table with backside shakers: the instruments in a, the restrained thin plate in b and the 2 shakers in c.

system for 3D dynamic measurements in stroboscopic coherent laser light, and in the Dantecdynamics Q-450, for 3D dynamic DIC acquisitions by means of hi-speed cameras (Nanosense Mk III) in high frequency & power white light.

It was clear since the beginning that there were differences in both spatial and frequency domains (more details in [13]). For the physics of each instrumentation see instead [27–31]. In particular, ESPI was plenty of spatial resolution (even 1 million dofs) with very clean datasets [13, 14, 16], but required stepped sine excitation, up to many kHz, resulting in a long and cumbersome data acquisition, especially if all the needed frequency lines were tightly spaced, as in the TEFFMA project. Great attention was paid to understand the limits & requirements of all these technologies in order to find a common intersection of measurements conditions: there resulted a promising compromise in the range [20 - 1024] Hz, with the 3 techniques having their own spatial and frequency resolutions. The linearity was checked by some comparative test with varying input power, to be able to compare measurements done at three different source power levels.

3.2 Brief experimental set-up description

The experimental set-up was designed in order to let all the three measurement technologies focus on the same dynamic behavior, as this was decided to be populated by a high modal density inside the frequency range of interest. An aluminum rectangular thin plate was tightened by wires, fixed to a solid frame on the air-spring optical table (see Fig.1) to restrain excessive rigid body movements. The surface of the plate was sprayed with a random noise pattern paint layer to full-fill the requirements of DIC. The excitation was given by electrodynamic shakers positioned on the back side of the plate, to full-fill the stepped-sine acquisition procedure for dynamic ESPI measurements and the requirements for SLDV and DIC. LMS Test.Lab drove the excitation in SLDV and DIC measurements, while ESPI system used an external sine waveform generator, synchronised with the phase-shifting procedures. To be able to calculate the *receptance* FRFs as in Eq.1, force signal was sampled at the shaker-plate interfaces by means of the force cell in the impedance heads.

3.3 Pre-testing the rig for optimal results

As already explained in [13], the tuning of the set-up went far beyond the traditional selection of the best acquisition parameters for each technology, being ESPI in the bunch of the techniques. ESPI permitted unprecedented fine tuning of the rig, by means of a precise adjustment of the nuts on the restraints, when the dynamic analysis was carried out at much higher frequencies than those in the common overlapping. ESPI strongly helped in assessing, fixing and thus preventing unwanted vibrations from any part of the rig up to 6500 Hz, just above the Nyquist frequency for SLDV: this means that the output motion of the plate was highly coherent with the input force [6, 12, 13], for the best achievable measurements.

Great attention was also paid to the optical alignments of all the instruments, in all the directions/rotations; also the depth of field of each optics was accurately selected to match the structural dynamics' requirements, in terms of collected photons and dynamic range for the best image quality.

The gained experience with full-field optical measurements revealed itself, together with the extended practice of photography of the author[2], as pivotal in arranging the multiple camera acquisition for photogrammetry [31] tests in [32, 33].

3.4 Estimating full-field FRFs from optical measurements

Once the methodology above is defined, *receptance FRF maps* at specific frequencies and excitation sources can be obtained as in Section 2. The interested reader can widen the understanding in [12, 13], to appreciate the spatial consistency & continuity of the data, with clean shapes, sharp nodal lines and excellent *Coherence*, especially from ESPI. The latter was here used as the most clean source available of experimental data for the specific purpose of deriving *strain FRFs* and *risk index maps*, as follows.

4 Deriving new quantities from full-field *receptances*

The high quality of the *receptance maps* obtainable from full-field optical techniques, especially from ESPI, in terms of field continuity and limited noise, deserves further investigations for novel derivative quantities by means of advanced numerical derivations, starting from *highly detailed strain maps*, as also underlined recently in [16].

4.1 Dynamic Strain FRFs

The *full-field generalized strain FRFs* can be obtained in each map location and frequency line by means of a robust differential operator (see in particular the Appendix of [16]) working on the *receptance map* $\mathbf{H_d}(x, y, \omega)$ along $\boldsymbol{q}$ directions, as follows for *in-plane* related contributions, where $i = x$, $k = y$:

$$\varepsilon_\omega(x,y)_{ik} = \frac{1}{2}\left(\frac{\partial \mathbf{H_d}(x,y,\omega)_i}{\partial q_k} + \frac{\partial \mathbf{H_d}(x,y,\omega)_k}{\partial q_i}\right). \tag{4}$$

To be noted is that, in the TEFFMA project, the contributions from Eq.4 were below the sensitivity threshold, therefore disregarded.

Instead, the *strain tensor* components due to *out-of-plane* bending-related displacements of the plate of thickness s were of relevance and were evaluated by:

$$\begin{aligned} &\varepsilon_\omega(x,y)_{xx_b} = -\frac{s}{2}\frac{\partial^2 \mathbf{H_d}(x,y,\omega)_z}{\partial x^2},\ \varepsilon_\omega(x,y)_{yy_b} = -\frac{s}{2}\frac{\partial^2 \mathbf{H_d}(x,y,\omega)_z}{\partial y^2}, \\ &\gamma_\omega(x,y)_{xy_b} = \gamma_\omega(x,y)_{yx_b} = -s\frac{\partial^2 \mathbf{H_d}(x,y,\omega)_z}{\partial x \partial y}. \end{aligned} \tag{5}$$

Lastly, the *Principal Strain FRF maps*, from both shakers, can be also obtained at each frequency line of the domain from the diagonalisation of the strain tensor in Eq.5, with a *complex-valued* data representation, to retain any phase relation coming from real test conditions on materials and boundaries. Therefore it becomes a complete characterization of the *experiment-based strain distribution* over the sensed surface in densely populated spatial and frequency domains.

4.2 Dynamic Stress FRFs

The introduction of a linear isotropic constitutive model, with its material parameters (E elastic modulus, ν Poisson ratio, G shear modulus, Λ Lamé constant) populated by the properties of the tested sample (here an

[2]Fine art, nature and wildlife photography at `https://www.colorazeta.it/index_EN.htm`

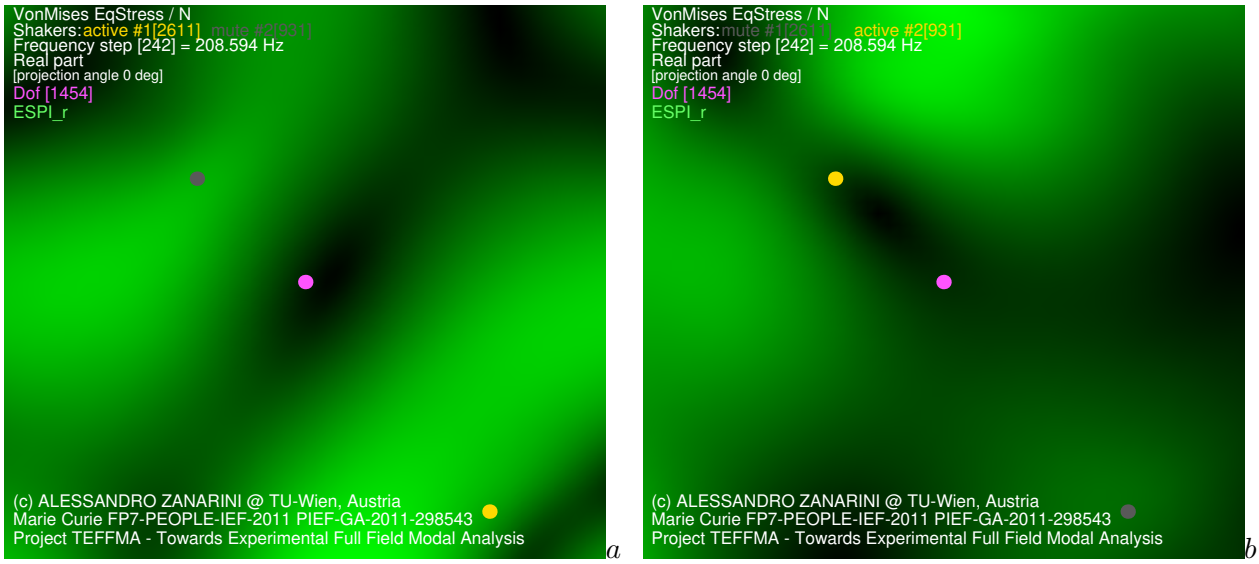

Figure 2: Examples of *Von Mises equivalent stress FRF maps* from optical techniques, direct experimental impedance models at 209 Hz, ESPI examples: from shaker 1 in a, from shaker 2 in b.

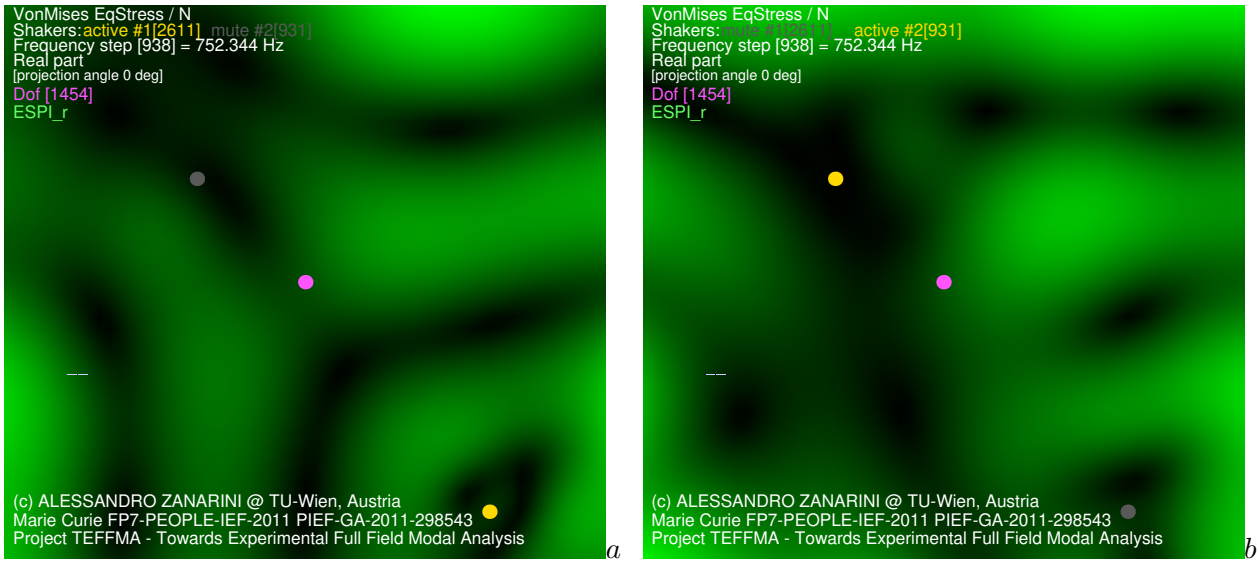

Figure 3: Examples of *Von Mises equivalent stress FRF maps* from optical techniques, direct experimental impedance models at 752 Hz, ESPI examples: from shaker 1 in a, from shaker 2 in b.

aluminium plate, as in Fig.1b), permits the evaluation of the *Stress FRF tensor* components from the *Strain FRFs* in Eq.5:

$$\begin{aligned} \sigma_\omega(x,y)_{ii} &= 2G\varepsilon_\omega(x,y)_{ii} + \Lambda\left(\varepsilon_\omega(x,y)_{xx} + \varepsilon_\omega(x,y)_{yy}\right) \\ \sigma_\omega(x,y)_{ij} &= 2G\varepsilon_\omega(x,y)_{ij} \\ G = E/2\left(1+\nu\right); \Lambda &= E\nu/\left(\left(1+\nu\right)\left(1-2\nu\right)\right) \end{aligned} \tag{6}$$

Therefore, with the constitutive model of any specific material (anisotropic and locally linearised included), also the *experiment-based Principal Stress FRF maps* can be evaluated from the *full-field receptances*, again by means of the diagonalisation of the *stress tensor* coming from Eq.6.

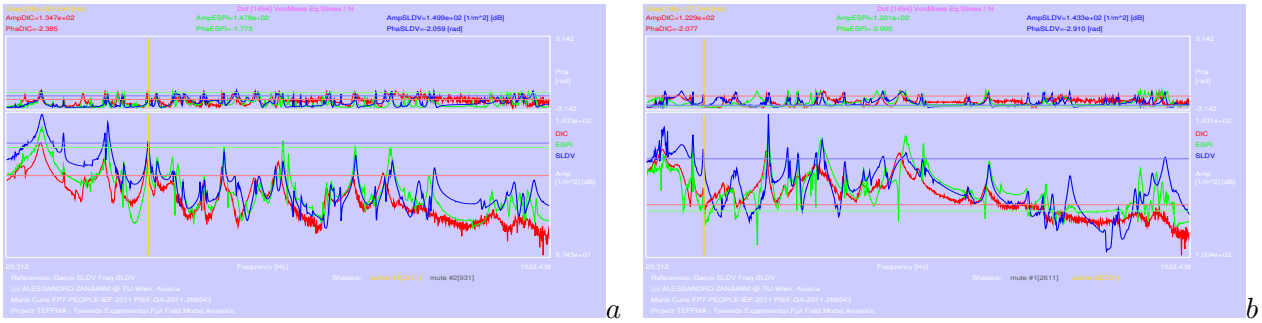

Figure 4: Examples of *Von Mises equivalent stress FRF graphs* from optical techniques, direct experimental impedance models in the 20-1024 Hz range, DIC-ESPI-SLDV examples at dof 1454: from shaker 1 in a, from shaker 2 in b.

5 Cumulative damage in fatigue life assessment

The extensive usage of such a broad set of detailed *experiment-based Stress FRF maps* opens new perspectives in material and component strength predictions from real life loading conditions. Plus, the frequency domain nature of *experiment-based full-field FRFs* becomes ideal when coupled with *fatigue spectral methods* for high cycles fatigue: the cumulative damage can be evaluated, once the dynamic signature of the excitation is known, across the whole sensed surface with *unprecedented quality and mapping ability* in the frequency and spatial domain, without any FE model.

5.1 Spectral methods in brief

Thanks to the *complex-valued* data representation of *experiment-based full-field FRFs*, the cumulative damage estimation can be approached by means of any *spectral method* (e.g. in [34]) in each location (x, y) of the maps, working on the structural stress response to the specific excitation.

Any *spectral method* targets the evaluation of an *equivalent range of stress cycles* $S_{eq}(x, y)$ in the entire frequency domain of interest, position dependent, representative of the damage inferred across the sensor locations by the whole *complex-valued spectrum* of the retained dynamics. This clearly means that the whole process can be characterized, in this paper, only by test-based quantities, without any FE model, as Eq.6 gives the *experiment-based Stress FRF maps*, to be coupled with real-life loading estimations in the frequency domain, with inherent *phase* variability.

Generally a criterion is defined in the equivalence among different structural stress states [35]: the *Von Mises equivalent stress*, even if quite simple, is widely used. The *power spectral density (PSD)* of *Von Mises equivalent stress* is crucial in any *spectral method*; it is evaluated from the excitation signature and the *Von Mises equivalent stress FRFs*, here rendered in the maps at 2 distinct single frequencies in Figs.2-3 and in single dof graphs of Fig.4, from both shakers. It is manifest just from these few pictures how the spatial patterns are changing in the frequency domain and are sensible to the excitation location, due to the complex structural dynamics designed for the sample in the TEFFMA project [13]. Important to note is also that the *experiment-based full-field stress FRFs* are usable with any other spectral method (see e.g. [34]), in particular those that retain the phase relations in the frequency domain, for further comparative works.

Therefore many *spectral methods* are based on $m_k = \int_0^\infty f^k PSD_{VM}(\omega) d\omega$, the *k-th order moments* of the frequency by the *PSD* of *Von Mises equivalent stress* $PSD_{VM}(\omega)$, from which we can obtain other parameters, such as the *effective frequency* $F_{zerocrossing} = F_{zc} = \sqrt{m_2/m_0}$, the *expected number of peaks per unit time* $F_{peaks} = F_p = \sqrt{m_4/m_2}$, and the *irregularity factor* $\gamma = \gamma_2 = F_{zc}/F_p = m_2/\sqrt{m_0 m_4}$, which may be used in the specific receipt of the selected *spectral method*.

a *b*

Figure 5: Examples of *white noise Von Mises equivalent stress PSD* graphs from optical techniques, direct experimental impedance models in the 20-1024 Hz range, DIC-ESPI-SLDV examples in dof 1947: from shaker 1 in a, from shaker 2 in b.

5.1.1 The parameters in the Dirlik's semi-empirical spectral method

The *Dirlik's semi-empirical spectral method* in [22] was here implemented, among the many available (see [34]), as it gives a sound prediction of the fatigue life for wide frequency band spectra of stress responses, as can be obtained by means of *experiment-based full-field FRFs*, combining the factors in Eq.7:

$$\begin{aligned}&\chi_m = (m_1/m_0)\,(m_2/m_4)^{1/2}\,; D_1 = 2\left(\chi_m - \gamma^2\right)/\left(1+\gamma^2\right); R = \left(\gamma - \chi_m - D_1^2\right)/\left(1-\gamma-D_1+D_1^2\right)\\ &D_2 = \left(1-\gamma-D_1+D_1^2\right)/\left(1-R\right); D_3 = 1-D_1-D_2; Q = 1.25\left(\gamma - D_3 - D_2 R\right)/D_1.\end{aligned} \tag{7}$$

The final receipt of the *Equivalent Range of Stress Cycles* $S_{eq}(x,y)$, evaluated across all the dofs (x,y) of the maps, raised to b fatigue strength exponent in the *Dirlik's semi-empirical spectral method* reads as:

$$S_{eq}^b = D_1(2\sqrt{m_0}Q)^b\Gamma(b+1) + (2^{3/2}\sqrt{m_0})^b\Gamma(1+b/2)[D_2R^b + D_3]. \tag{8}$$

There follows the *Time-to-failure distribution*, expressed in seconds $[s]$, function of $S_{eq}(x,y)$ from Eq.8, of the *expected number of peaks per unit time* $F_p(x,y)$, and of the K_r fatigue strength coefficient and b exponent for the specific material of the loaded sample:

$$T_{failure}(x,y) = K_r/\Big(F_p(x,y)S_{eq}^b(x,y)\Big). \tag{9}$$

5.1.2 Coloured noise excitation for the Frequency-to-failure evaluation

New *Von Mises equivalent stress PSDs* are easily evaluated from the *Von Mises equivalent stress FRFs*, when changing the *excitation signature*, as also in [10, 12, 16]. All the *Von Mises equivalent stress FRFs*, here called $H_{VM}(\omega,x,y)$ and obtained from Eq.6, are multiplied by the spectrum $F_{C_\alpha}(\omega)$ of the excitation force to obtain the peculiar cycle ranges of *complex-valued* stress $S_r(\omega,x,y)$:

$$S_r(\omega,x,y) = H_{VM}(\omega,x,y)F_{C_\alpha}(\omega). \tag{10}$$

Under the linearity assumption, the *PSD of the Von Mises equivalent stress* $PSD_{VM}(\omega,x,y)$, responsible of the cumulated damage, can be obtained with $()^*$ as *complex-valued* conjugate operator and $\Delta\omega$ as the frequency interval:

$$PSD_{VM}(\omega,x,y) = S_r(\omega,x,y)S_r^*(\omega,x,y)/\Delta\omega. \tag{11}$$

For a clear output of these fundamental and methodological researches, an input source, shaped as coloured noise, was adopted; instead, being this procedure applied to specific production samples that face real life loading conditions, the peculiar test spectrum need to be used as the excitation, as in [36]. It is in Eq.10 where *complex-valued* spectra can introduce effects related to phase delays among the components on the structural dynamics of the system. The amplitude spectrum of the coloured noise $F_{C_\alpha}(\omega)$, here used as the

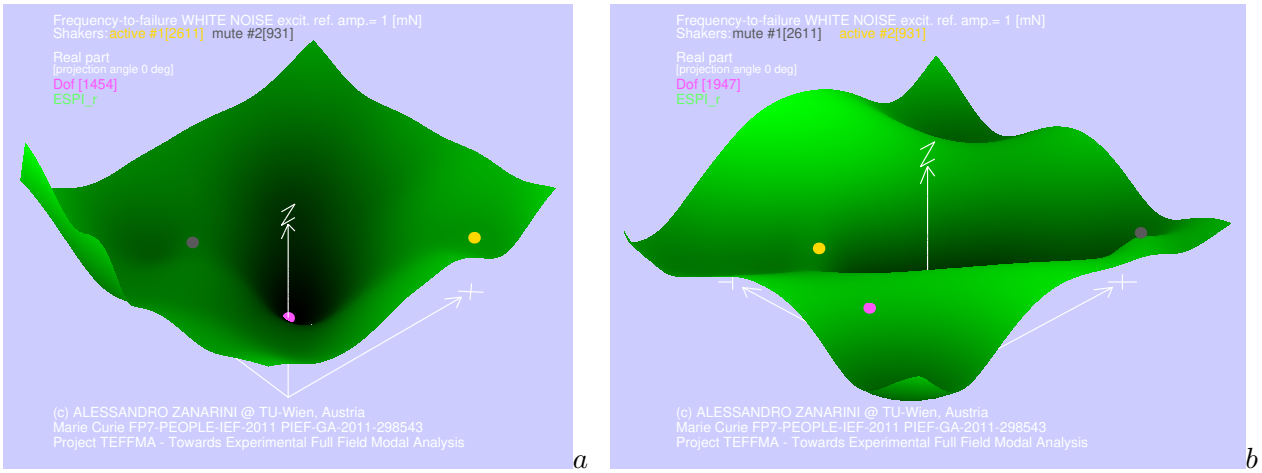

Figure 6: Examples of *frequency-to-failure distribution* maps from *white noise excitation*, ESPI examples: from shaker 1 in a, from shaker 2 in b.

force excitation, can be simply modelled as a real valued function in the ω frequency, yielding:

$$F_{C_\alpha}(\omega) = \frac{F_0}{(\omega)^\alpha} \tag{12}$$

with $\alpha \in [-2, 2]$ defining the noise color ($\alpha = -2$ for *violet noise*, $\alpha = -1$ for *blue noise*, $\alpha = 0$ for *white noise*, $\alpha = 1$ for *pink noise* and $\alpha = 2$ for *red noise*) and with F_0 intended as the reference amplitude of the excitation force in the frequency range. No specific assumptions on the relative phase among the components on the frequency axis were made, thus the phases were kept fixed to null delay for all the lines by means of real numbers. The use of *complex-valued* input spectra changes only the product in Eq.10, being all the quantities then complex-valued. Therefore a *red noise* highly exalts the lower frequency region of the *Von Mises equivalent stress FRFs*, a *white noise* gives the same energy to all the frequency lines and a *violet noise* gives a strong power to the higher frequency structural dynamics, with the *pink noise* and *blue noise* as intermediate situations, aside of the neutral *white noise*, here adopted for an equal energy balance in all the frequency lines. While examples of $H_{VM}(\omega, dof_{1454})$ are plotted in Fig.4 at dof 1454 from both shakers, in the whole 20-1024 Hz frequency domain, in Fig.5 the $PSD_{VM}(\omega, dof_{1947})$ are plotted in dof 1947 when a *white noise excitation* is used with $F_0 = 0.001$ N, which does not change the shape of the corresponding $H_{VM}(\omega, dof_{1947})$, but scales the latter. The structural dynamics in the 1454 & 1947 dofs will be later useful to understand the fatigue life and risk index results.

It can also be of interest to define the reciprocal of Eq.9, what can be called the *Frequency-to-failure* $F_{failure}(x, y)$, expressed in [1/s] or [Hz] and defined as

$$F_{failure}(x, y) = \Big(F_p(x, y) S^b_{eq}(x, y)\Big)/K_r, \tag{13}$$

to highlight where the failure should start first, as in Fig.6 by brighter tones on higher log Z axis. Of interest for this specific paper is how the change in the excitation point affects the whole *frequency-to-failure* distribution, underlining the importance of the right estimation of the loading conditions in real-life applications.

6 Defect tolerance based on full-field dynamic testing & Risk Index

In the high-cycles fatigue the results from Eq.9 give a very high number of seconds, with a mean value in the broad range of 10^8-10^{13}, as from [12]. The *Hours_to_Failure* can be easily defined in every *dof* of location (x, y) as:

$$Hours\_to\_Failure_{[dof]} = HtF_{[dof]} = T_{failure_{[dof]}}/3600. \tag{14}$$

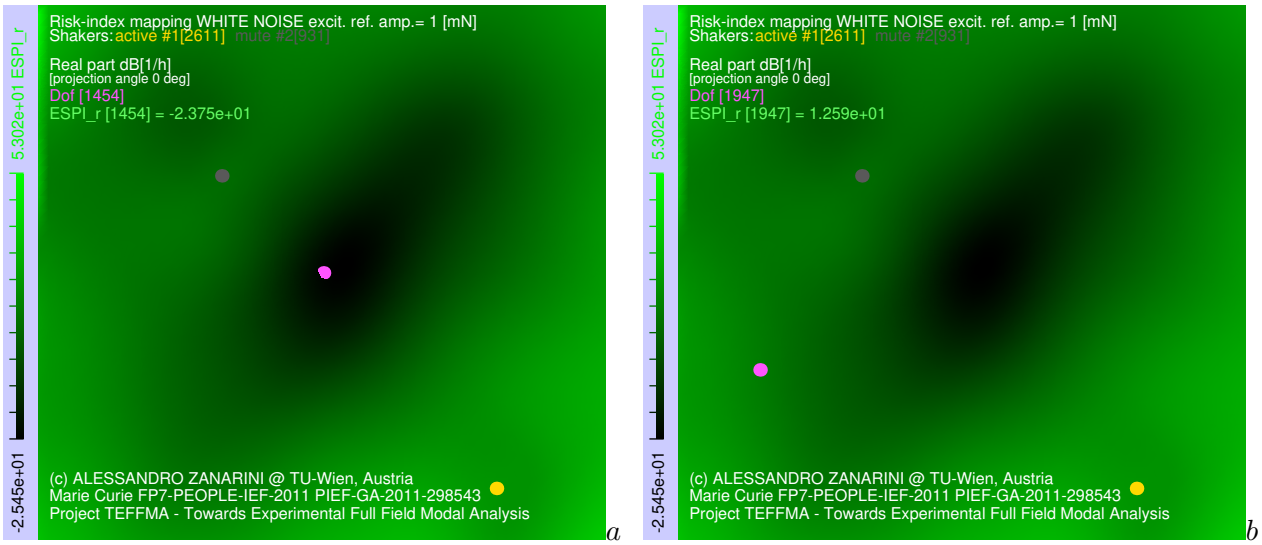

Figure 7: Examples of *Risk Index mapping* in dof 1454 in a and 1947 in b, with *white noise excitation* from shaker 1. If $threshold = 11$, a defect in dof 1454 is tolerable, whereas a defect in dof 1947 is intolerable, above the selected threshold of acceptance, thus dangerous.

With the *experiment-based Hours-to-Failure maps* in Eq.14 a *defect tolerance concept* can be introduced and numerically exemplified, as better detailed in [25], with great impact perspectives in manufacturing as well as in exercise, based on the real dynamics of the part and a *Risk Index* definition of specific choice. Therefore, working with the evaluations from the *fatigue spectral methods* on experimental full-field data, a ***Risk Index*** can be proposed, which is based on the *Hours_to_Failure* and can be defined in every dof, in a decibel shape, relative to the *mean* of *HtF* distribution in the whole field:

$$RiskIndex_{[dof]} = 20log_{10}(\frac{1}{HtF_{[dof]}}) - 20log10(\frac{1}{HtF_{mean}}). \tag{15}$$

Therefore the *defect tolerance* can be here said to be proportional to the defined *Risk Index*, putting a *threshold* of acceptance: **defect tolerance** α **Risk Index**, e.g. the safety is achieved when $RiskIndex_{[dof]} \leq threshold$. This means that, once the *Risk Index* and the *threshold* are defined, each defect that is found in a region whose *Risk Index* is below the *threshold* can be considered tolerable for the specific task of the part. On the contrary, any region whose *Risk Index* is above the *threshold* can not tolerate the presence of any defect, with clear repercussions in quality assurance checks both in manufacturing and in life-long maintenance.

The *defect tolerance concept* can be utilized by means of any excitation, as the different *coloured noise excitation* coming from Eq.12, or also by a *real measured force* spectrum, to evaluate the related *VonMises equivalent stress PSDs* of Eq.11. Therefore different *PSDs* bring their respective *Risk Index maps*, as well as with different excitation injection points, due to the different structural responses.

The *damage location assessment* on real components may play a relevant role under specific *defect tolerance strategies*. The chosen 2 dofs above were just a virtual example, but the same ESPI-based *NDT* shown in paper [24] may give a *real defect distribution map*, which can be the input in *Risk Index maps*, here obtained by ESPI full-field dynamic testing as in [23], both for production & exercise of our parts. In this coupled strategy, the real location of the defect can tell if it can be accepted or not, in manufacturing or exercise, once the real structural dynamics and excitation signature are fully known. Therefore the *NDT*, the *structural dynamics'* measurement and the *defect tolerance criteria* can all be based on *full-field dynamic testing*, to put the most advanced experimental structural dynamics' knowledge into higher safety targets.

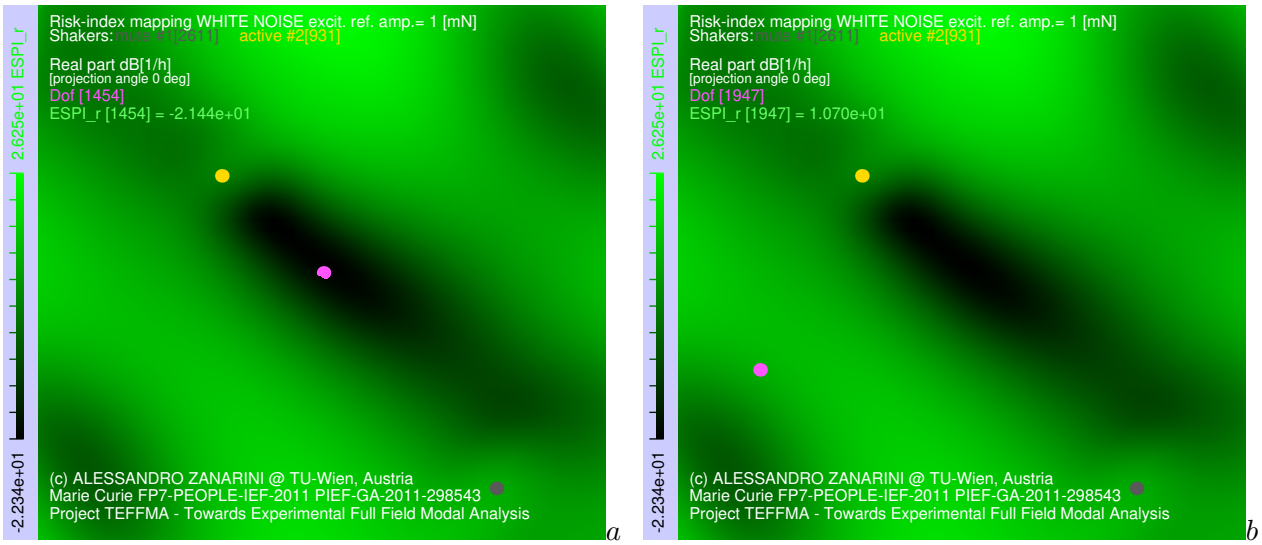

Figure 8: Examples of *Risk Index mapping* in dof 1454 in a and 1947 in b, with *white noise excitation* from shaker 2. If $threshold = 11$, defects in both dofs 1454 and 1947 are tolerable, though a defect in dof 1947 appears close to the selected threshold of acceptance.

6.1 *Defect tolerance concept* with *white noise* excitation in 2 different locations

To proficiently explore the effect of the excitation location, the same *white noise* amplitude spectrum, fixed null phase among frequency lines' components, was adopted; the same *Risk Index* definition of Eq.15, with a *threshold* $= 11$, is evaluated across the spatial domains; instead, the 2 shakers of the TEFFMA project, with their respective chain of *receptance maps'* processing, where used.

In the examples of Fig.7-8 the location of the magenta dof, with a *threshold* of 11, gives the information if, according to the proposed *Risk Index*, the potential defect is tolerable or not, with clear safety repercussions in production or exercise. The 2 dofs are those previously mentioned in Section 5: 1454 and 1947 on this grid, the former at the center of the sample, the latter on the lower left side, where the dynamic responses proved to be much stronger across the frequency domain. While dof 1454 is located, according to the threshold of acceptance adopted, in a safe region for a potential defect, for the position of dof 1947 - thanks to the complete experiment-based structural dynamics, the specific white noise excitation signature and the risk index mapping - it can be stated that the acceptance of a defect is indeed conditioned upon the excitation point selection. Which means in these examples that a potential defect in dof 1947 of the sensed grid, under white noise excitation, is tolerable only when the energy in the structure is injected by shaker 2, whereas is dangerous, not tolerable, if the excitation comes from shaker 1. Furthermore, the risk index mapping suggests a grading room of this defect tolerance concept, tunable by means of the threshold, as in dof 1947 the risk index with white noise from shaker 2 is 10.7, below, but quite close to the threshold's value of 11. But further discussions, with evidence from other colured noises or excitation spectra, exceed the scope of this article.

There resulted quite interesting outputs, confirming how the *experiment-based full-field structural dynamics* is fully retained and can usefully represent the loaded structures in broad frequency band dynamics, without assumptions, nor modal identification errors nor specific damping simplifications.

All this to underline the effectiveness of *full-field FRF based Risk Index mapping*: it was sufficient to change the *dynamic signature* of the excitation to understand how the problematic areas on the sample changed, with the complete structural dynamics of the real test, with the specific blending of modal shapes as appeared in the test set-up, but without modal identification's approximation. It might be underlined therefore how strategic becomes to run experiments in the same operative conditions of the real samples, as all this knowledge contributes to the final acceptance of potential defects into the components.

7 Conclusions

This paper has highlighted the importance of *enhanced experiment-based tools* in bringing the real and complete structural dynamics of a component in a broad frequency band, together with excitation signature and energy injection location, into fatigue life predictions. Furthermore, the concept of *defect tolerance* has been introduced as based upon the fatigue life predictions obtained from *full-field experiment-based receptances*. The definition of a *Risk Index* with related *acceptance threshold* was used to discriminate the dangerous location of potential defects, once the real dynamic behavior is fully retained, and not simplified, directly from real samples and without any FE model to be carefully updated.

The experimental optical full-field measurement techniques are becoming a viable means for a *risk tolerance assessment* in production and working conditions, because of their ability to identify defects, of their unprecedented mapping ability and of their retention of a refined *complex-valued* structural dynamics in both the frequency and spatial domain, to be coupled with direct estimations of real-life loading conditions.

Acknowledgements

This activity is a spin-off of the Project TEFFMA - Towards Experimental Full Field Modal Analysis, funded by the European Commission at the Technische Universitaet Wien, through the Marie Curie FP7-PEOPLE-IEF-2011 PIEF-GA-2011-298543 grant, for which the Research Executive Agency is greatly acknowledged. TU-Wien, in the person of Prof. Wassermann and his staff, are kindly acknowledged for having hosted the TEFFMA project of the author at the *Schwingungs- und Strukturanalyse* / Optical Vibration Measurement Laboratory. The workstation used, to extensively code the numerical tools and to process the datasets, was provided by the author on his own savings.

References

[1] A. Zanarini, "Dynamic behaviour carachterization of a brake disc by means of electronic speckle pattern interferometry measurements," in *Proceedings of the IDETC/CIE ASME International Design Engineering Technical Conferences & Computers and Information in Engineering Conference, Long Beach, California, USA, September 24-28*. ASME, 2005, pp. 273–280, paper DETC2005-84630. [Online]. Available: https://doi.org/10.1115/DETC2005-84630

[2] A. Zanarini, "Damage location assessment in a composite panel by means of electronic speckle pattern interferometry measurements," in *Proceedings of the IDETC/CIE ASME International Design Engineering Technical Conferences & Computers and Information in Engineering Conference, Long Beach, California, USA, September 24-28*. ASME, 2005, pp. 1–8, paper DETC2005-84631. [Online]. Available: https://doi.org/10.1115/DETC2005-84631

[3] A. Zanarini, "Full field ESPI measurements on a plate: challenging experimental modal analysis," in *Proceedings of the XXV IMAC, Orlando (FL) USA, Feb 19-22*. SEM, 2007, pp. 1–11, paper s34p04. [Online]. Available: https://www.researchgate.net/publication/266896551_Full_field_ESPI_measurements_on_a_plate_Challenging_Experimental_Modal_Analysis

[4] A. Zanarini, "Fatigue life assessment by means of full field ESPI vibration measurements," in *Proceedings of the ISMA2008 Conference, September 15-17, Leuven (Belgium)*, P. Sas, Ed. KUL, 2008, pp. 817–832, Condition monitoring, Paper 326. [Online]. Available: https://doi.org/10.13140/RG.2.1.3452.9365

[5] A. Zanarini, "Full field ESPI vibration measurements to predict fatigue behaviour," in *Proceedings of the IMECE2008 ASME International Mechanical Engineering Congress and Exposition, October 31- November 6, Boston (MA) USA*. ASME, October 31- November 6 2008, pp. 165–174, paper IMECE2008-68727. [Online]. Available: https://doi.org/10.1115/IMECE2008-68727

[6] A. Zanarini, "On the estimation of frequency response functions, dynamic rotational degrees of freedom and strain maps from different full field optical techniques," in *Proceedings of the ISMA2014 including USD2014 - International Conference on Noise and Vibration Engineering, Leuven, Belgium, September 15-17*. KU Leuven, September 15-17 2014, pp. 1177–1192, Dynamic testing: methods and instrumentation, paper ID676. [Online]. Available: http://past.isma-isaac.be/downloads/isma2014/papers/isma2014_0676.pdf

[7] A. Zanarini, "On the role of spatial resolution in advanced vibration measurements for operational modal analysis and model updating," in *Proceedings of the ISMA2014 including USD2014 - International Conference on Noise and Vibration Engineering, Leuven, Belgium, September 15-17*. KU Leuven, September 15-17 2014, pp. 3397–3410, Operational modal analysis, paper ID678. [Online]. Available: http://past.isma-isaac.be/downloads/isma2014/papers/isma2014_0678.pdf

[8] A. Zanarini, "Comparative studies on full field FRFs estimation from competing optical instruments," in *Proceedings of the ICoEV2015 International Conference on Engineering Vibration, Ljubljana, Slovenia, September 7-10*. Univ. Ljubljana & IFToMM, September 7-10 2015, pp. 1559–1568, ID191. [Online]. Available: https://www.researchgate.net/publication/280013709_Comparative_studies_on_Full_Field_FRFs_estimation_from_competing_optical_instruments

[9] A. Zanarini, "Accurate FRFs estimation of derivative quantities from different full field measuring technologies," in *Proceedings of the ICoEV2015 International Conference on Engineering Vibration, Ljubljana, Slovenia, September 7-10*. Univ. Ljubljana & IFToMM, September 7-10 2015, pp. 1569–1578, ID192. [Online]. Available: https://www.researchgate.net/publication/280013778_Accurate_FRF_estimation_of_derivative_quantities_from_different_full_field_measuring_technologies

[10] A. Zanarini, "Full field experimental modelling in spectral approaches to fatigue predictions," in *Proceedings of the ICoEV2015 International Conference on Engineering Vibration, Ljubljana, Slovenia, September 7-10*. Univ. Ljubljana & IFToMM, September 7-10 2015, pp. 1579–1588, ID193. [Online]. Available: https://www.researchgate.net/publication/280013788_Full_field_experimental_modelling_in_spectral_approaches_to_fatigue_predictions

[11] A. Zanarini, "Model updating from full field optical experimental datasets," in *Proceedings of the ICoEV2015 International Conference on Engineering Vibration, Ljubljana, Slovenia, September 7-10*. Univ. Ljubljana & IFToMM, September 7-10 2015, pp. 773–782, ID196. [Online]. Available: https://www.researchgate.net/publication/280013876_Model_updating_from_full_field_optical_experimental_datasets

[12] A. Zanarini, "Broad frequency band full field measurements for advanced applications: Point-wise comparisons between optical technologies," *Mechanical Systems and Signal Processing*, vol. 98, pp. 968 – 999, 2018. [Online]. Available: https://doi.org/10.1016/j.ymssp.2017.05.035

[13] A. Zanarini, "Competing optical instruments for the estimation of Full Field FRFs," *Measurement*, vol. 140, pp. 100 – 119, 2019. [Online]. Available: https://doi.org/10.1016/j.measurement.2018.12.017

[14] A. Zanarini, "Full field optical measurements in experimental modal analysis and model updating," *Journal of Sound and Vibration*, vol. 442, pp. 817 – 842, 2019. [Online]. Available: https://doi.org/10.1016/j.jsv.2018.09.048

[15] A. Zanarini, "On the making of precise comparisons with optical full field technologies in NVH," in *Proceedings of the ISMA2020 including USD2020 - International Conference on Noise and Vibration Engineering, Leuven, Belgium, September 7-9*. KU Leuven, September 7-9 2020, pp. 2293–2308, Optical methods and computer vision for vibration engineering, paper ID 695. [Online]. Available: https://www.researchgate.net/publication/344353185_On_the_making_of_precise_comparisons_with_optical_full_field_technologies_in_NVH

[16] A. Zanarini, "Chasing the high-resolution mapping of rotational and strain FRFs as receptance processing from different full-field optical measuring technologies," *Mechanical Systems and Signal*

Processing, vol. 166, p. 108428, 2022. [Online]. Available: https://doi.org/10.1016/j.ymssp.2021.108428

[17] W. Heylen, S. Lammens, and P. Sas, *Modal Analysis Theory and Testing*, 2nd ed. Leuven (Belgium): Katholieke Universiteit Leuven, 1998, ISBN 90-73802-61-X.

[18] W. Liu and D. Ewins, "The Importance Assessment of RDOF in FRF Coupling Analysis," in *Proceedings of the IMAC 17th Conference, Kissimmee, Florida*, 1999, pp. 1481–1487, Society for Experimental Mechanics (SEM). [Online]. Available: http://www3.imperial.ac.uk/pls/portallive/docs/1/49146.PDF

[19] Research network, "QUATTRO Brite-Euram project no: BE 97-4184," European Commision Research Framework Programs, Tech. Rep., 1998.

[20] D. J. Ewins, *Modal Testing - theory, practice and application*, 2nd ed. Baldock, Hertfordshire, England: Research Studies Press Ltd., 2000. [Online]. Available: https://www.wiley.com/en-it/Modal+Testing%3A+Theory%2C+Practice+and+Application%2C+2nd+Edition-p-9780863802188

[21] M. Friswell and J. E. Mottershead, *Finite Element Model Updating in Structural Dynamics*, ser. Solid Mechanics and Its Applications. Kuwler Academic Publishers, Springer Netherlands, 1995.

[22] T. Dirlik, "Application of computers in fatigue analysis," Ph.D. dissertation, University of Warwick, January 1985. [Online]. Available: http://wrap.warwick.ac.uk/2949/

[23] A. Zanarini, "On the defect tolerance by fatigue spectral methods based on full-field dynamic testing," *Procedia Structural Integrity*, vol. 37, pp. 525–532, 2022, paper ID 105, ICSI 2021 The 4th International Conference on Structural Integrity. [Online]. Available: https://doi.org/10.1016/j.prostr.2022.01.118

[24] A. Zanarini, "On the exploitation of multiple 3D full-field pulsed ESPI measurements in damage location assessment," *Procedia Structural Integrity*, vol. 37, pp. 517–524, 2022, paper ID 104, ICSI 2021 The 4th International Conference on Structural Integrity. [Online]. Available: https://doi.org/10.1016/j.prostr.2022.01.117

[25] A. Zanarini, "Introducing the concept of defect tolerance by fatigue spectral methods based on full-field frequency response function testing and dynamic excitation signature," *International Journal of Fatigue*, vol. 165, p. 107184, 2022. [Online]. Available: https://doi.org/10.1016/j.ijfatigue.2022.107184

[26] A. Zanarini, "On the approximation of sound radiation by means of experiment-based optical full-field receptances," in *Proceedings of the ISMA2022 including USD2022 - International Conference on Noise and Vibration Engineering, Leuven, Belgium, September 12-14*. KU Leuven, September 12-14 2022, pp. 1–15, paper ID 207.

[27] P. K. Rastogi, *Optical Measurement Techniques and Applications*. Nordwood, MA 02062, U.S.A.: Artech House, Inc., 1997.

[28] T. Kreis, *Handbook of Holographic Interferometry*. Berlin, Germany: Wiley-VCH, 2004.

[29] M. S. Allen and M. W. Sracic, "A new method for processing impact excited continuous-scan laser doppler vibrometer measurements," *Mechanical Systems and Signal Processing*, vol. 24, no. 3, pp. 721 – 735, 2010. [Online]. Available: https://doi.org/10.1016/j.ymssp.2009.11.004

[30] D. Di Maio and D. J. Ewins, "Continuous scan, a method for performing modal testing using meaningful measurement parameters; Part I," *Mechanical Systems and Signal Processing*, vol. 25, no. 8, pp. 3027 – 3042, 2011. [Online]. Available: https://doi.org/10.1016/j.ymssp.2011.05.018

[31] J. Baqersad, P. Poozesh, C. Niezrecki, and P. Avitabile, "Photogrammetry and optical methods in structural dynamics - A review," *Mechanical Systems and Signal Processing,* , 2016, Elsevier Science Ltd. [Online]. Available: https://doi.org/10.1016/j.ymssp.2016.02.011

[32] R. Del Sal, L. Dal Bo, E. Turco, A. Fusiello, A. Zanarini, R. Rinaldo, and P. Gardonio, "Vibration measurements with multiple cameras," in *Proceedings of the ISMA2020 including USD2020 - International Conference on Noise and Vibration Engineering, Leuven, Belgium, September 7-9*. KU Leuven, September 7-9 2020, pp. 2275–2292, Optical methods and computer vision for vibration engineering, paper ID 481.

[33] R. Del Sal, L. Dal Bo, E. Turco, A. Fusiello, A. Zanarini, R. Rinaldo, and P. Gardonio, "Structural vibration measurement with multiple synchronous cameras," *Mechanical Systems and Signal Processing*, vol. 157, p. 107742, 2021. [Online]. Available: https://www.sciencedirect.com/science/article/pii/S0888327021001370

[34] T. Dirlik and D. Benasciutti, "Dirlik and Tovo-Benasciutti Spectral Methods in Vibration Fatigue: A Review with a Historical Perspective," *Metals*, vol. 11, no. 9, 2021. [Online]. Available: https://www.mdpi.com/2075-4701/11/9/1333

[35] J. Papuga, M. Margetin, and V. Chmelko, "Various parameters of the multiaxial variable amplitude loading and their effect on fatigue life and fatigue life computation," *Fatigue & Fracture of Engineering Materials & Structures*, vol. 44, no. 10, pp. 2890–2912, 2021. [Online]. Available: https://onlinelibrary.wiley.com/doi/abs/10.1111/ffe.13560

[36] P. Wolfsteiner and S. Sedlmair, "Deriving gaussian fatigue test spectra from measured non gaussian service spectra," *Procedia Engineering*, vol. 101, pp. 543 – 551, 2015, 3rd International Conference on Material and Component Performance under Variable Amplitude Loading, VAL 2015, Editors J. Papuga and M. Ruzicka.

Appendix

A Nomenclature

DIC	Digital Image Correlation
dof	degree of freedom
EFFMA	Experimental Full Field Modal Analysis
EMA	Experimental Modal Analysis
ESPI	Electronic Speckle Pattern Interferometry
FRF	Frequency Response Function
NDT	Non Destructive Testing
NVH	Noise and Vibration Harshness
ODS	Operative Deflection Shape
SLDV	Scanning Laser Doppler Vibrometer
(ω)	frequency dependency
$\mathbf{X}(\omega)$	displacement map
$\mathbf{F}(\omega)$	excitation forces
$\mathbf{H_d}(\omega)$	*Receptance* map